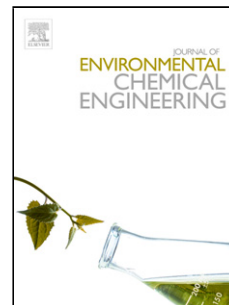


Accepted Manuscript

Title: Efficient and Reusable Iron-Zinc Oxide Catalyst for Oxidative Desulfurization of Model Fuel

Authors: Wafaa Abdul-Kadhim, Mohd Asyrak Deraman, Syamsul Bahari Abdullah, Saiful Nizam Tajuddin, Mashitah Mohd. Yusoff, Yun Hin Taufiq-Yap, Mohd Hasbi Ab. Rahim



PII: S2213-3437(17)30093-3
DOI: <http://dx.doi.org/doi:10.1016/j.jece.2017.03.001>
Reference: JECE 1507

To appear in:

Received date: 29-12-2016
Revised date: 27-2-2017
Accepted date: 1-3-2017

Please cite this article as: Wafaa Abdul-Kadhim, Mohd Asyrak Deraman, Syamsul Bahari Abdullah, Saiful Nizam Tajuddin, Mashitah Mohd. Yusoff, Yun Hin Taufiq-Yap, Mohd Hasbi Ab. Rahim, Efficient and Reusable Iron-Zinc Oxide Catalyst for Oxidative Desulfurization of Model Fuel, Journal of Environmental Chemical Engineering <http://dx.doi.org/10.1016/j.jece.2017.03.001>

This is a PDF file of an unedited manuscript that has been accepted for publication. As a service to our customers we are providing this early version of the manuscript. The manuscript will undergo copyediting, typesetting, and review of the resulting proof before it is published in its final form. Please note that during the production process errors may be discovered which could affect the content, and all legal disclaimers that apply to the journal pertain.

Efficient and Reusable Iron-Zinc Oxide Catalyst for Oxidative Desulfurization of Model Fuel

Wafaa Abdul-Kadhim^{1,2}, Mohd Asyrak Deraman¹, Syamsul Bahari Abdullah³, Saiful Nizam Tajuddin¹, Mashitah Mohd. Yusoff¹, Yun Hin Taufiq-Yap⁴, Mohd Hasbi Ab. Rahim^{1,5*}

¹*Faculty of Industrial Sciences & Technology, Universiti Malaysia Pahang, Lebuhraya Tun Razak, Gambang, 26300, Pahang, Malaysia.*

²*Oil Technology, University of Technology, Baghdad, Iraq*

³*Faculty of Chemical Engineering & Natural Resources, Universiti Malaysia Pahang, Lebuhraya Tun Razak, Gambang, 26300, Pahang, Malaysia.*

⁴*Catalysis Science and Technology Research Centre, Faculty of Science, Universiti Putra Malaysia, 43400 Serdang, Selangor, Malaysia*

⁵*Automotive Engineering Centre (AEC), Universiti Malaysia Pahang, Pekan Campus, 26600, Pekan, Pahang, Malaysia*

***Corresponding author:** mohdhasbi@ump.edu.my

Highlights

- The Fe-ZnO catalyst is reusable without prior regeneration steps.
- Synergistic effect of Fe and ZnO facilitate the removal of sulphur.
- High sulfur removal without altering the hydrocarbon structure.
- Synthesis of Fe-ZnO using sol-gel technique without the use of surfactants.

Abstract

In this study, Fe-ZnO catalyst synthesized via modified sol-gel technique with different Fe doping ratio (2, 3, and 5) wt % was explored for oxidative desulfurization (ODS) of model fuel. The sol-gel technique was adopted without the use of surfactants. The catalysts were characterized by several means of characterization techniques (TGA, XRD, FTIR, N₂-physisorption, XPS, FESEM-EDX and NH₃-TPD). The characterization results clearly showed that sol-gel technique is a suitable method to synthesize highly crystalline metal oxide materials with smaller particle size, higher surface area and tunable acidic properties. The ODS reaction conditions and Fe metal loading were found to influence the dibenzothiophene (DBT) removal efficiency. The catalytic ODS data showed that Fe-ZnO with 5 wt % of Fe catalyst is capable in total removal of DBT within shorter reaction time under mild reaction conditions in the presence of H₂O₂ as an oxidant. The catalyst is reusable for six consecutive cycles of reaction without regeneration steps and the characteristic of spent catalyst was confirmed with XRD and FTIR analysis. The close catalytic cycle involving H₂O₂ as an oxidant was shown through proposed mechanistic pathway.

Keywords: *Oxidative Desulfurization; Fe-ZnO; Sol-Gel; Fuel; Hydrogen Peroxide*

1. Introduction

Desulfurization techniques were developed since the early 40's where hydrodesulfurization (HDS) procedure was adopted through the use of Co-Mo or Ni-Mo catalysts[1]. The HDS process involved high pressure and temperature that contributed to higher operating cost. Besides, it is a non-selective process and its limited capability in removing refractory sulfur compounds such as dibenzothiophene and benzonaphthothiophenes that exist in the fuel which reduced the possibility to obtain ultra-low sulfur fuel, *i.e.* Euro V with less than 10 ppm of sulfur [2]. Later on, several techniques for diesel desulfurization were suggested to enhance the performance of the sulfur removal such as bio-desulfurization [3-5], extractive desulfurization [6], alkylation based desulfurization [7], selective adsorption and oxidative desulfurization [8, 9]. Each aforementioned techniques possess own advantages and weaknesses. For example, it is impossible to achieve ultra-low level of sulfur by using either extractive or adsorptive desulfurization alone [10]. Thus, the combination of the techniques is preferred and one of them is two-step process involving oxidative desulfurization (ODS) followed by extraction of oxygenated sulfur using polar solvent. On top of that, ODS is capable in removing the widest possible sulfur compounds due to the nature of reaction as well as the ability to operate under mild operating conditions with the presence of green oxidants [11, 12].

Common oxidants utilized for ODS are hydrogen peroxide (H_2O_2) and tertiary butyl hydroperoxide (TBHP) either alone or combined with acid such acetic acid, benzoic acid, formic acid, or butanoic acid [13]. The usage of acid is not preferable since it will reduce the quality of fuel. Besides, there are several solid catalyst that have been tested for ODS reaction such as heteropoly acid, either alone or supported [14-16], and metal oxides, *i.e.* oxides of (Mo, Mn, Sn, Fe, Co, Zn) metals [17-19]. However, most of it either involved complex and

multistep synthesis method or unrecyclable. Nevertheless, the well-studied metal oxides material such as zinc oxide and iron oxide that were synthesized using relatively simple, fast and environmental friendly technique can be fine-tuned and suitable criteria for catalytic purpose can be obtained. Iron oxide for example, has the ability to activate a considered clean oxidant such as H_2O_2 that produced active superoxide/peroxide species [20] while the ZnO was reported for adsorptive desulfurization by Adeyi et al [21]. They found that ZnO is able to remove the sulfur content without changing the main hydrocarbon structure where non-sulfur-containing crude fuel oil mass remains unchanged. Thus, the combination of adsorptive capability of zinc oxide and oxidant activated by iron oxide will enhance the possibility in efficient removal of refractory sulfur compound through ODS technique. Indeed, there is no available report on utilizing mixed iron-zinc oxide catalyst for ODS reaction. In addition to that, iron-zinc oxide material was reported in the literature to have both hydrophobic-hydrophilic characteristic [20]. Therefore, it has a great potential to act like phase-transfer catalyst, in which it is further important for the reaction that consists of immiscible H_2O_2 containing H_2O and hydrocarbon solution.

In the present work, Fe-ZnO is formulated as a new catalyst for ODS catalytic reaction. The sulfur removal efficiency has been tested using simulated fuel oil solution made of dibenzothiophene (DBT) dissolved in *n*-heptane. For record, many simulated ODS studies reported in literature had utilized *n*-heptane as model hydrocarbon [22, 23]. The aim of the present work is to develop a reusable heterogeneous catalyst that performs high sulfur removing efficiency without affecting the hydrocarbon molecular structure.

2. Experimental

2.1 Materials

Zinc acetate dihydrate (99.5 %), iron (III) nitrate nanohydrate (98.8 %) and oxalic acid (99.5 %) supplied by Friendemann Schmidt Chemical were used for the catalyst preparation. The simulated fuel oil was made of *n*-heptane and dibenzothiophene, DBT (98 %) (R&M chemicals). Hydrogen peroxide 30% in H₂O (Merck) was used as oxidizing agent.

2.2 Catalyst Preparation

Fe-ZnO nanoparticles with different Fe loading (2, 3 and 5 wt %) were prepared using a modified sol-gel method. Prior to the synthesis, the calculated amount of zinc acetate, iron nitrate and oxalic acid were dissolved in ethanol with 100, 20, 50 mL respectively. Then, the prepared zinc acetate solution was heated under reflux oil bath at 70 ± 5 °C controlled by a temperature controller for 30 minutes with vigorous continuous stirring. Iron precursor was added drop-wise into Zn solution followed by drop-wise addition of oxalic acid until the gel is obtained. The resulted gel is stirred continuously for 1 hour before being filtered, washed with acetone and water, followed by drying at 100 °C for 4 hours. Finally, the product was calcined under static air at 450 °C for 30 minutes.

2.3 Catalyst Characterization

The thermogravimetric analysis (TGA) (METTLER TOLEDO) was used to study the thermal behavior of the prepared catalysts. X-ray diffraction (XRD) (Rigaku, Miniflex II) patterns were recorded from 10° to 80° with a scanning rate of 0.2°/s. FTIR spectrometry (Perkin-Elmer, Spectrum 100) was used to identify the functional group over the range of 400-4000 cm⁻¹. Specific surface area of the synthesized sample was analyzed using Micromeritics Asap 2020. The morphology of catalyst produced was observed using Field Emission

Scanning Electron Microscopy (FESEM) (JEOLEVO-50, Japan) equipped with Energy Dispersive X-Ray analysis (EDX). The surface analysis of the Fe-ZnO samples was carried out using ULVAC-PHI Quantera II (Ulvac-PHI, INC.) X-ray photoelectron spectrometer, using monochromatic Al-K α ($h\nu = 1486.6$ eV) as the excitation source. In details, wide scan analysis was performed using a pass energy of 280 eV with 1 eV per step and narrow scan was performed using a pass energy of 112 eV with 0.1 eV per step. Prior to de-convolution, charge correction was performed at C 1s by setting binding energies of C-C and C-H to 284.8 eV. Thermo TPDRO 1100 instrument was used to analyze acidic properties of prepared catalysts using NH₃-TPD methods. Approximately, 50 mg of sample was placed in a reaction tube and treated for 1 h at 200 °C under a nitrogen flow of 20 mL/min. Then, the sample was dosed with NH₃, again at 20 mL/min. After dosing, the samples were cooled to 50 °C then heated up to 900 °C at 10 °C/min, under helium flow of 20 mL/min.

2.4 Catalytic reaction

In a typical run, solution containing 2000 ppm dibenzothiophene (DBT) in *n*-heptane was used as a simulated solution of fuel oil. The oxidative desulfurization experiment was performed in a three-necked 250 mL round-bottomed flask equipped with a condenser fitted with magnetic stirrer and immersed in an oil bath controlled by a temperature controller (Scheme 1). (H₂O₂, 30 % in H₂O) as oxidant and calculated amount of catalyst. The catalyst and H₂O₂ were introduced once the temperature attained at 80 °C under atmospheric pressure for a time period of 1 hour at high stirring rate of 700 rpm. The reaction solution was sampled at specific sampling time. The liquid sample was then transferred to a separating funnel followed by the addition of extraction solvent (acetonitrile) and mixed thoroughly. The

hydrocarbon layer of simulated oil solution is then separated subjected to qualitative and quantitative analysis.

2.5 Analysis of product

The hydrocarbon part of liquid reaction after extraction was subjected into two different analysis methods for the purpose of validation and verification. In this case, the routine and main technique used to determine the efficiency of DBT removal was gas chromatography (GC) (Agilent Technologies 7693) equipped with a flame ionization detector (FID) and DB-Wax capillary column (60 m, 0.25mm, 0.25 μ m). Helium was used as a carrier gas with flow rate of 1.3 mL/min. The oven was held at 80 °C for 2 minutes while the injector and detector temperature were maintained at 250 °C. The removal percentage of DBT is calculated based on equation 1 [24]. Average relative standard deviations (RSD) for all catalytic data are found to be less than 5 %.

$$(\%) = \frac{C_0 - C_t}{C_0} \times 100 \quad (1)$$

Where C_0 is the sulfur (DBT) initial concentration in the simulated oil solution and

C_t is the sulfur concentration of the oil phase after reaction time (t).

In addition to GC-FID analysis, the hydrocarbon solution after reaction was also subjected to ATR-FTIR (Perkin-Elmer, Spectrum 100) in order to qualitatively determine and validate the presence of oxygenated sulfur (sulfoxide and sulfone) compound.

2.6 Analysis of H₂O₂ remain after reaction

The amount of unreacted H₂O₂ for selected reactions was analytically determined by the titration technique of aqueous phase of extracted simulated oil solution after reaction against potassium permanganate solution of known normality (N). Specifically, 1 mL of the reaction product solution is transferred to a conical flask, then the solution was diluted with 10 mL of deionized water followed by the addition of diluted sulfuric acid (1:5 sulfuric acid to water ratio). Finally, the solution was titrated with potassium permanganate solution (0.1 N). The used volume of the potassium permanganate was measured when the colour of the solution become faint pink.

The following relation (equation 2) is used to determine the unreacted H₂O₂ volume:

$$N_1 V_1 = N_2 V_2 \quad (2)$$

Where N_1V_1 , is normality and volume of potassium permanganate respectively, N_2V_2 is normality and volume of reaction solution.

2.7 Catalyst reusability

After the completion of the reaction, the reaction solution above the solid catalyst was completely decanted. Then, a fresh solution of the required volume of *n*-heptane containing DBT was added and the reaction was repeated in the presence of similar amount of newly added H₂O₂ solution.

In order to analyze any possibility of metal components leach-out into the reaction medium, the decanted liquid was analyzed for possible leached metals using ICP-MS Agilent 7500 series. The amounts of metal leach-out can be calculated and compared to the actual amount of metal available in catalyst prior to the reaction.

3. Results and Discussion

3.1 Catalyst Characterization

3.1.1. Thermal stability (TGA–DTG)

The thermal stability of ZnO and 5 wt % Fe-ZnO nanoparticles was studied using TGA–DTG analysis. Fig. 1 (a and b) shows the resultant curves for both ZnO and 5 wt% Fe-ZnO prepared samples using the similar method. The DTG displayed first endothermic peak below 160 °C that corresponds to the evaporation of remaining water. The second peak is ascribed to the thermal decomposition of oxalate for the ZnO and 5 wt % Fe-ZnO.

The TGA curves of the samples showed that there were two different stages of weight loss for the complete decomposition of zinc oxalate. The first weight loss of approximately 15 % and 20 % for ZnO and 5 wt % Fe-ZnO respectively occurs between 110 and 160 °C. This weight loss was attributed to the removal of water from zinc oxalate dihydrate, which has a reported theoretical water content of approximately 14 %. The second stage of heating from 360 to 420 °C resulted in a larger weight loss of approximately 42 % and 39 % for ZnO and 5 wt % Fe-ZnO respectively. The weight loss can be attributed to the complete decomposition of zinc oxalate dihydrate into zinc oxide, which is close to the theoretical value [19, 20]. The difference in weight loss between ZnO and 5 wt % Fe-ZnO samples is due to the thermal decomposition of the additional iron nitrate in the doped ZnO [21]. No further weight loss was observed by TGA at temperature higher than 410 °C. This temperature is the point at which the thermal analysis of ZnO and 5 wt % Fe-ZnO oxalate dihydrate has been completed.

3.1.2. X-ray Diffraction (XRD)

Fig. 2 shows the X-ray diffraction patterns of ZnO and ZnO doped with different Fe loading (2, 3, and 5 wt %). Three main diffraction peaks were observed at 31.7° , 34.4° , and 36.4° that correspond to polycrystalline wurtzite structure of ZnO for all samples with diffraction data also showed good agreement with ICDD powder diffraction file for ZnO (No-10800075). The ZnO structure does not change after doping with (2, 3 and 5 wt %) Fe, suggesting the formation of single phase Fe-ZnO material. The diffraction spectrums of the doped Fe-ZnO samples did not show any existence of Fe_2O_3 . This might be a result of the high dispersion of Fe^{3+} into the lattice of ZnO crystal or due to the small amount of Fe^{3+} used in doping [25, 26].

On the contrary, the XRD peaks of Fe-ZnO were found broad in correlation with the undoped ZnO peaks, suggesting that the Fe doping into the lattice of ZnO inhibited the crystallization of samples that resulted to lattice disorder and stresses. This phenomenon happened because of the difference in ionic sizes of the Fe^{3+} (0.067 nm) and Zn^{2+} (0.083 nm) ions [27]. In case of 5wt % Fe-ZnO., two additional peaks were observed at 35.3° and 42.9° in the diffraction pattern and identified as $\alpha\text{-Fe}_2\text{O}_3$ peaks [28]. A small shift was observed in the position of main peak (1 0 1) to the lower side of 2θ value due an increase in the radius of Fe^{+3} compared to Zn^{+2} , signifying the substitution of Fe atoms over Zn atoms. Similar observation was observed on other transition metals (Mn, Cu, and Ni) doped ZnO as reported by Ekambaram et al., and Dinesha et .al [29, 30].

The Scherer's formula [31] was used to calculate the mean crystallite size of the Fe-ZnO nanoparticles which was observed to be decreased from 36 to 16 nm due to an increase in the Fe percentage in sample as specified by Muneer et al [32].

3.1.3 BET Surface Area

BET surface area of Fe-ZnO is increased by increasing the amount of loaded Fe (Table 1). The observed trend is in good agreement with the crystallite size calculated from XRD data where smaller ZnO particles were obtained with presence of higher Fe loading. Scherer's formula was used to calculate crystallite size [33].

$$D = \frac{K \lambda}{\beta \cos \theta} \quad \dots \quad \dots \quad \dots \quad (3)$$

Where D is crystallite size, k is shape factor or Scherer constant (0.89), λ is the X-ray wavelength for Cu α , β is the peak broadening at half maximum and θ is the Bragg angle.

The N₂ adsorption–desorption isotherms for ZnO and Fe-ZnO samples are shown in Fig. 3 all the nitrogen adsorption-desorption isotherms of the samples are found to be of Type IV in nature as per the IUPAC classification and exhibited a H4 hysteresis loop, which is typical of mesopores solids; consisting of larger mesopores [34, 35].

3.1.4 Fourier Transform-Infra Red (FTIR)

Fig. 4 shows the FTIR results for ZnO and Fe-ZnO. The band at 3419 to 3438 cm⁻¹ agrees to the stretching vibration of –OH bond. These stretching vibrations classify the water molecule on the surface of sample [36]. This can be due to the formation of metal hydroxides as an intermediate compound before the formation of ZnO. The C=O stretching peak between 1550 and 1690 cm⁻¹ and the asymmetric stretching of the C–O between 1300 and 1390 cm⁻¹ are also evident [31]. The band observed in 3d at 2345 cm⁻¹ is attributed to C=O stretching mode, which is possibly due to the absorption of CO₂ from air by the metallic cation [37, 38]. The absorption band observed at 420–430 cm⁻¹ in FTIR spectra is associated with the vibrational mode characteristic of Zn–O bonding [39]. In addition, the spectrum of Fe–O

nanoparticles was exhibited of vibration at 660-670 cm^{-1} and that is similar with Madejová study [40].

3.1.5 Field Emission Scanning Electron Microscope with EDX (FESEM-EDX)

Surface morphology of ZnO and Fe-ZnO with different Fe loading are illustrated in Fig. 5. It can be seen from the micrograph that Fe-ZnO shows similar morphology as ZnO. Although all set of catalysts show sphere in-shape, the sphere particle for doped samples are closely connected as straight line-structure. On top of that, close observation on each sphere particle disclosed similar trend of particle size which further support the BET and XRD data.

Energy dispersive X-ray (EDX) analysis was conducted on the Fe-ZnO samples to determine the wt % of the Fe in the samples respectively. It is evident that the doped Fe into ZnO results is in good agreement with theoretical wt % of the Fe content in the samples. The percentage composition of each element quantified using EDX analysis is shown in Table 2.

3.1.6 X-Ray Photoelectron Spectroscopy (XPS)

Fig. 6a elucidated the presence of hematite ($\alpha\text{-Fe}_2\text{O}_3$) in all Fe-ZnO samples. The XPS peak assignment of hematite phase was based on Fe ($2p_{3/2}$) and Fe ($2p_{1/2}$) peaks observed at range of 710 eV and 724 eV respectively [16, 41]. The presence of clear satellite peak around 719 eV justify the availability of Fe^{3+} species; whereas the occurrence of Fe^{2+} is negligible due to unobservable of satellite peak correspond to Fe^{2+} at 715 eV. Besides, unavailability of metallic Fe is confirmed by close observation at 706 eV of Fe ($2p_{3/2}$), which is the signature peak of Fe^0 [42] thus confirming the XRD data that only Fe_2O_3 is present in all Fe-ZnO (2, 3, 5 wt %) loading catalyst. The high resolution spectra of the Zn species in the Fe-ZnO

catalysts (2, 3, 5 wt %) loading (Fig.6b) show a characteristic binding energy at ~1021 eV (Zn 2p_{3/2}) that correspond to Zn²⁺ bonded to O in ZnO. The slight shift in peak position towards higher energy can be attributed to the introduction of Fe into ZnO. The deconvolution of O 1s peak of all the Fe-ZnO samples (Figures 6c₁, 6c₂, and 6c₃) revealed the presence of three oxygen species. The lower binding energy (~529 eV) can be assigned to O-Zn or O-Fe whereas the peak at ~531eV corresponds to Zn-OH or Fe-OH bonds. The existence of different M-OH bonds or chemisorbed water is less significant since very low intensities were observed at binding energy of ~532.4 eV [43].

3.1.7 Temperature Programmed Desorption (NH₃-TPD)

The NH₃-TPD test was used to obtain the quantitative amounts of acid sites for ZnO and ZnO doped with Fe at three different weights loading respectively. The distribution peak is classified into (T<200 °C) as weak, (200 °C - 400 °C) as medium, and (T>400 °C) as strong acid sites [44]. The result of the NH₃-TPD test indicated an increase in the acidic sites of ZnO doped with Fe as compared to ZnO (Fig. 7 and Table 3). Indeed, similar trend is observed by increasing the Fe doping, which increases the availability and strength of adsorption sites.

3.2 Catalytic Testing

3.2.1 Effect of Fe metal loading on Fe-ZnO catalyst

Fig. 8 shows the effect of Fe-ZnO with different iron loading on the DBT removal efficacy. Synergistic effect between Zn and Fe was observed in improving removal of DBT, in which both single ZnO and Fe₂O₃ gave lower DBT removal. The efficiency of sulfur removal was found to increase by increasing the Fe content and it is believed due to the availability of Fe=O catalytic sites that are responsible in activating iron superoxide for oxidation reaction. Even XPS analysis of all samples illustrates the presence of oxygen bonded

iron that is more significant for 5 wt% Fe loading catalyst. Besides, the efficiency of Fe-ZnO is further improved by adsorptive capability of ZnO that assist in increasing the possible contact between DBT with catalyst active sites. Indeed, the introduction of Fe particles to ZnO resulted in creating smaller particles with an average crystallite size of 16 nm when compared to the initial ZnO particles size (36 nm) and thus will contribute to the increment of the contact surface area of the catalyst, which subsequently increasing the sulfur removal efficiency. It is important to note here that the catalytic data only showed limited DBT removal in the absence of catalyst. The DBT removal efficiency increases with the increase of doping ratio due to higher acidic sites as observed from the NH_3 -TPD analysis. Interaction between H_2O_2 and acidic sites of the catalyst improves the electrophilic attack of H_2O_2 on DBT as weak nucleophile, forming intermediary per-oxometallic complex on the catalyst surface.

3.2.2 Effect of reaction time

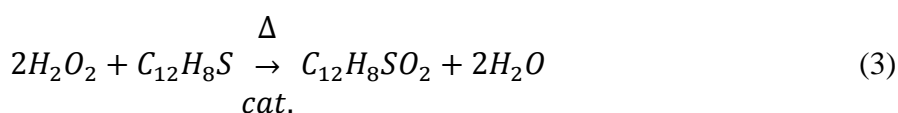
The catalytic data in Fig. 9 clearly show that the DBT removal efficiency increases with an increment of reaction time. However, insignificant sulfur removal was witnessed after 60 minutes of reaction time exceeding to longest tested time; 240 min. It is anticipated that at prolong reaction time more than 60 min, it does not have much effect on the proportion of desulfurization due to the degradation of most oxidant. Quantitative analysis through titration method discovered that most of H_2O_2 were utilized after reaction, either through selective utilization or unselective utilization due to (i) decomposition to oxygen and water, (ii) hydrogenation to water and (iii) direct non-selective formation of water [44].

3.2.3 Effect of reaction temperature

Fig. 10 shows that the sulfur removal efficiency is affected by reaction temperature. An increase in reaction temperature from 30 to 80 °C will increase removal efficiency of sulfur from the simulated oil till it reaches 68.2 ± 3.1 % at 80 °C. The maximum operation temperature chosen was 80 °C due to the fact that the simulated fuel oil (*n*-heptane) is evaporated at higher temperatures. Besides, high temperature will initiate non-selective decomposition of H₂O to produce O₂ and H₂O, subsequently suppress the oxidation capability [45-47]. Availability of the H₂O₂ throughout the reaction is crucial since it will form an active species which is capable of oxidizing sulfur to sulfoxide and sulfone. Similar range of temperature is operated by other catalytic systems and it mainly due to the similar reason. Indeed, comparable trend of sulfur removal efficiency with increment of reaction temperature was observed [47, 48]. It can be stated that increasing the temperature will increase the internal energy between the molecules and that will enhance the rapid molecular movement, which will result in increasing the removal efficiency.

3.2.4 Effect of oxidant concentration

Fig.11 shows the effect of the oxidizing agent (H₂O₂) to sulfur content ratio (O/S) on the separation efficiency. The results show that the removal efficiency increases by increasing the O/S ratio until O/S of 4 mol ratios is reached, which is higher than the reaction stoichiometry with maximum DBT removal of 92.7 ± 3.7 % as shown in equation 3.



Further increase in the oxidant content will result in decreasing the DBT removal efficiency. An increased of H₂O₂ mol ratio could cause unproductive decomposition of H₂O₂ to O₂ and H₂O and that will definitely reduce the oxidation efficiency. Besides, the presence

of water produced in high quantity will affect the oxidation process. It is important to highlight that during the oxidation process, few bubbles were observed when fresh catalyst is immersed in the DBT solution, indicating the presence of O_2 gas originated from decomposition of hydrogen peroxide. The amount of H_2O_2 calculated at the end of the reaction showed almost total used of H_2O_2 .

3.2.5 Effect of catalyst mass

Fig.12 illustrates that the DBT removal efficiency is increased by increasing the catalyst weight loading and reaching the maximum removal percentage of 92.6 ± 3.2 % when the weight of the catalyst is 50 mg. Further increase in the catalyst weight resulted in decline of the DBT removal efficiency; up to 66.8 ± 2 % at a catalyst weight of 75 mg. This decrease in efficiency is attributed to an agglomeration and aggregation effect, which reduced the number of active sites on catalyst surface hence reducing the effective surface area. Besides, the presence of Fe in relatively high amount will trigger the unproductive decomposition of H_2O_2 .

. 3.2.6 ODS reaction at optimize reaction condition

In order to improve the removal of DBT, the optimization of reaction parameters is carried out in the presence of most active catalyst, 5 wt % Fe-ZnO. It was established that the total removal of DBT can be achieved by performing the reaction at optimized conditions of 80 °C for 60 minutes with O/S 4 mol ratio of H_2O_2 and 50 mg weight of catalyst.

Catalytic activity comparison with other heterogeneous catalyst is crucial in order to evaluate the ODS efficiency of newly develop Fe-ZnO catalytic material. For that reason, the catalytic reaction rate needs to be calculated. In this case, the catalytic reaction rate (v_t) is

calculated based on the equation 4 stated by W. Zhang et al [49] and it was defined as the mass of sulfur converted per unit mass of catalyst per unit time ($\text{mg S mg}^{-1} \text{ min}^{-1}$).

$$v_t = \frac{M_S}{t * M_{cat}} \quad (4)$$

Where v_t is the catalytic reaction rate, M_S is the mass of the sulfur converted within the reaction time of t , and M_{cat} is the mass of a catalyst.

Based on the ODS catalytic data using Fe-ZnO catalyst, the catalytic reaction rate (v_t) is calculated for the reaction carried out at 80 °C for 60 minutes with O/S 4 mol ratio of H_2O_2 and 12.5 mg weight of catalyst, in which produced 92.7 % DBT removal. Thus, provides the v_t value of $2.47 \text{ mg S mg}^{-1} \text{ min}^{-1}$. It was important to note that the v_t obtained from this study is comparable or higher than most related works. For example, Zhang et al [45] with HPW/ ZrO_2 - SiO_2 catalyst only produced $0.033 \text{ mg S mg}^{-1} \text{ min}^{-1}$ whereas only $0.007 \text{ mg S mg}^{-1} \text{ min}^{-1}$ v_t obtained by Caero et al [50] for the ODS reaction in the presence of Mo oxides on alumina catalyst.

3.3 Catalyst Reusability Study

The catalyst reusability study was carried out under the optimized reaction conditions. The catalyst after reaction was recovered through decantation. Then, the decanted catalyst is used for the new reaction with the addition of the same amount of H_2O_2 and simulated oil solution followed by catalytic reaction under similar conditions. The present work proved the fact that the investigated catalysts can be recycled at least up to 6 cycles with an unremarkable decrease in activity as shown in Fig.13.

The reusable trend observed for Fe-ZnO catalyst is supported by the characterization of spent catalyst through XRD and FTIR analysis. It can be seen from XRD diffractogram (Fig 14) and FTIR spectrum (Fig. 15) that the spent catalyst had retained XRD pattern of fresh catalyst in which it is confirmed that the characteristic of catalyst remain unchanged after ODS reaction. In specific, in (Fig. 14) the presence absorption bands in the region 1170–878 cm^{-1} becomes stronger due to organics capping of iron [37].

In addition, Table 4 shows the N_2 physisorption results of spent catalyst. The reduction in the efficiency is mainly ascribed as the reduction of the active sites on the catalyst surface. The rate reduction is possibly due to the formation of ‘ash layer’ that contributed to shrinking catalyst core thus it provides lower surface area for the reaction [51].

The stability of Fe-ZnO catalyst in ODS reaction is further supported by ICP-MS analysis of liquid sample after reaction. Agilent 7500 series was employed to calculate the amount of metal leach-out and compared to the actual amount of metal available in catalyst prior to the reaction. Only 0.8 % of Fe and 1.2 % of Zn were lost after 6 cycles of reaction.

3.4 Stability of fuel

The ability to remove the sulfur compound without altering the hydrocarbon structure is crucial in preserving the quality of fuel thus detail analysis on chromatogram of liquid hydrocarbon had been discovered and it confirmed the fact that Fe-ZnO catalyst is not affecting the main structure of the treated oil. In specific, Fig. 16 (a, b, c) compares the GC analysis graphs of the pure *n*-heptane and simulated oil before and after oxidation process. The figure shows clearly that the composition of the *n*-heptane was not changed after the oxidation process.

Besides, Fig.17 shows the ATR-FTIR spectra comparison between the DBT and oxidized DBT. Both compounds show almost identical bands, except that the two new bands with a strong intensity at nearly 925 cm^{-1} that can be assigned as the asymmetrical and symmetrical stretching vibration modes of sulfoxide [52] and medium band 1046 cm^{-1} corresponds to the S=O bond of sulfone [11, 53, 54]. Thus confirmed that the oxidation process successfully occurred and producing oxygenated sulfur compound.

3.5 Mechanistic study

The Fe-ZnO catalyst has shown to be efficient and reusable in removal of DBT compound. Thus, the possible catalytic pathway is proposed in (Scheme 2). It is believed that the reaction is initiated by nucleophilic attack of H_2O_2 by the Fe=O bond of Fe-ZnO catalyst surface, which had generated active intermediate iron peroxides. Then, nucleophilic attack of the sulfur atom with higher electron density in dibenzothiophene on iron peroxide is conducted to form sulfoxide and regenerated Fe=O where the sulfoxide later undergoes further oxidation by using iron peroxide that converts it to a corresponding sulfone and regenerated Fe=O for close cycle of reaction. The propose mechanism demonstrate that the presence of active Fe=O sites are important for an efficient ODS reaction. Thus, 5 wt % Fe-ZnO with bigger surface area, smaller crystallite size and higher amount of Fe justify the availability of more Fe=O sites compared to analogue catalyst with lower Fe loading.

4. Conclusions

The presence of sulfur compounds in the crude oil and its refinery products can massively affect the quality of the refinery products and its price. Besides that, the presence

of these compounds have huge environmental impact with all its known forms such as sulfates in atmosphere that can results in acid rain, sulfates (SO_4^{2-}) in water and sulfur dioxide from fuel combustion. The elimination of the sulfur compounds from the crude oil and its refinery products is an essential process due to its economic and environmental impact. In this study, intrinsically safe Fe-ZnO catalyst has been successfully synthesized and used in sulfur removal process through oxidative desulfurization reaction and H_2O_2 as green oxidant. The catalyst was prepared through modified sol-gel method without the use of surfactants and structurally tested by XRD, FTIR, N_2 -physisorption, FESEM-EDX and NH_3 -TPD. It was observed that the effect of increasing Fe doping concentration had produced Fe-ZnO with smaller crystallite size, higher surface area and increases the acidic active sites. It then provided synergistic effect in efficient removal of sulfur containing compound through ODS reaction. The Fe^{3+} was proposed to be responsible in activating the oxidant whereas the ZnO is believed to assist in adsorption thus it increases the probability of sulfur removal. The heterogeneous nature of catalyst was confirmed through catalytic reaction, characterization and leaching test of spent catalyst without additional catalyst regeneration steps. Besides, the hydrocarbon was verified to be stable under tested reaction conditions.

Acknowledgements

The authors are grateful for the internal research funding (RDU130317) from Universiti Malaysia Pahang, Kuantan, Malaysia.

References

- [1] C. Song, An overview of new approaches to deep desulfurization for ultra-clean gasoline, diesel fuel and jet fuel, *Catal. Today*, 86 (2003) 211-263.
- [2] D.J. Monticello, Biodesulfurization and the upgrading of petroleum distillates, *Curr. Opin. Biotech.*, 11 (2000) 540-546.
- [3] N. Tang, X. Zhao, Z. Jiang, C. Li, Oxidation of dibenzothiophene using oxygen and a vanadophosphate catalyst for ultra-deep desulfurization of diesels, *Chinese J. Catal.*, 35 (2014) 1433-1437.
- [4] B.H. Kim, H.Y. Kim, T.S. Kim, D.H. Park, Selectivity of desulfurization activity of *Desulfovibrio desulfuricans* M6 on different petroleum products, *Fuel Process Technol.*, 43 (1995) 87-94.
- [5] S. Guobin, X. Jianmin, Z. Huaiying, L. Huizhou, Deep desulfurization of hydrodesulfurized diesel oil by *Pseudomonas delafieldii* R-8, *J. Chem. Tech. Biot.*, 80 (2005) 420-424.
- [6] S. Zhang, Q. Zhang, Z.C. Zhang, Extractive desulfurization and denitrogenation of fuels using ionic liquids, *Ind. Eng. Chem. Res.*, 43 (2004) 614-622.
- [7] X. Wu, Y. Bai, Y. Tian, X. Meng, L. Shi, Gasoline desulfurization by catalytic alkylation over methanesulfonic acid, *Bull. Korean Chem. Soc.*, 34 (2013) 3055-3058.
- [8] B. Wang, J. Zhu, H. Ma, Desulfurization from thiophene by $\text{SO}_4^{2-}/\text{ZrO}_2$ catalytic oxidation at room temperature and atmospheric pressure, *J. Hazard Mater.*, 164 (2009) 256-264.
- [9] A. Nisar, J. Zhuang, X. Wang, Construction of amphiphilic polyoxometalate mesostructures as a highly efficient desulfurization catalyst, *Adv. Mater. (Weinheim, Ger.)*, 23 (2011) 1130-1135.
- [10] H. Rang, J. Kann, V. Oja, Advances in desulfurization research of liquid fuel, *Oil Shale*, 23 (2006) 164-176.
- [11] A.M. Dutta, B.K. Saikia, B.P. Baruah, Oxidative desulphurization of north-east indian coals by using different metal ions/oxides as catalyst, *Int. J. Innov. Res Dev*, 7 (2012) 214-220.
- [12] J.M. Campos-Martin, M.C. Capel-Sanchez, P. Perez-Presas, J.L.G. Fierro, Oxidative processes of desulfurization of liquid fuels, *J. Chem. Tech. Biot.*, 85 (2010) 879-890.
- [13] M. Shakirullah, W. Ahmad, I. Ahmad, M. Ishaq, Oxidative desulphurization study of gasoline and kerosene: Role of some organic and inorganic oxidants, *Fuel Process. Technol.*, 91 (2010) 1736-1741.
- [14] G.-N. Yun, Y.-K. Lee, Beneficial effects of polycyclic aromatics on oxidative desulfurization of light cycle oil over phosphotungstic acid (PTA) catalyst, *Fuel Process. Technol.*, 114 (2013) 1-5.
- [15] J. Xiao, L. Wu, Y. Wu, B. Liu, L. Dai, Z. Li, Q. Xia, H. Xi, Effect of gasoline composition on oxidative desulfurization using a phosphotungstic acid/activated carbon catalyst with hydrogen peroxide, *Appl. Energy*, 113 (2014) 78-85.
- [16] Y. Chen, S. Zhao, Y.-F. Song, An efficient heterogeneous catalyst based on highly dispersed $\text{Na}_7\text{H}_2\text{LaW}_{10}\text{O}_{36}\cdot 32\text{H}_2\text{O}$ nanoparticles on mesoporous silica for deep desulfurization, *Appl. Catal. B-Environ.*, 466 (2013) 307-314.
- [17] W.A.W.A. Bakar, R. Ali, A.A.A. Kadir, W.N.A.W. Mokhtar, Effect of transition metal oxides catalysts on oxidative desulfurization of model diesel, *Fuel Process Technol.*, 101 (2012) 78-84.
- [18] O. González-García, L. Cedeño-Caero, V-Mo based catalysts for oxidative desulfurization of diesel fuel, *Catal. Today*, 148 (2009) 42-48.

- [19] J.-X. Guo, L. Fan, J.-F. Peng, J. Chen, H.-Q. Yin, W.-J. Jiang, Desulfurization activity of metal oxides blended into walnut shell based activated carbons, *J. Chem. Tech. Biot.*, 89 (2014) 1565-1575.
- [20] U. Arellano, J.A. Wang, M.T. Timko, L.F. Chen, S.P. Paredes Carrera, M. Asomoza, O.A. González Vargas, M.E. Llanos, Oxidative removal of dibenzothiophene in a biphasic system using sol-gel FeTiO₂ catalysts and H₂O₂ promoted with acetic acid, *Fuel*, 126 (2014) 16-25.
- [21] A.A. Adeyi, F. Aberuagba, Comparative analysis of adsorptive desulphurization of crude oil by manganese dioxide and zinc oxide, *Res. J. Chem. Sci.*, 2 (2012) 14-20.
- [22] D. Serrano, R. Sanz, P. Pizarro, I. Moreno, S. Medina, Hierarchical TS-1 zeolite as an efficient catalyst for oxidative desulphurization of hydrocarbon fractions, *Appl. Catal. B-Environ.*, 146 (2014) 35-42.
- [23] M.A. Rezvani, M. Oveisi, M.A.N. Asli, Phosphotungstovanadate immobilized on PVA as an efficient and reusable nano catalyst for oxidative desulphurization of gasoline, *J. Mol. Catal. A-Chem.*, 410 (2015) 121-132.
- [24] Q. Tang, S. Lin, Y. Cheng, S. Liu, J.-R. Xiong, Ultrasound-assisted oxidative desulfurization of bunker-C oil using tert-butyl hydroperoxide, *Ultrason. Sonochem.*, 20 (2013) 1168-1175.
- [25] L. Huilian, Y. Jinghai, Z. Yongjun, Y. Lili, W. Maobin, D. Xue, Structure and magnetic properties of Fe-doped ZnO prepared by the sol-gel method, *J. Phys.-Condens. Matter*, 21 (2009) 145803.
- [26] P. Vijayan, C. Mahendiran, C. Suresh, K. Shanthi, Photocatalytic activity of iron doped nanocrystalline titania for the oxidative degradation of 2,4,6-trichlorophenol, *Catal. Today*, 141 (2009) 220-224.
- [27] A.K. Srivastava, M. Deepa, N. Bahadur, M.S. Goyat, Influence of Fe doping on nanostructures and photoluminescence of sol-gel derived ZnO, *Mater. Chem. Phys.*, 114 (2009) 194-198.
- [28] S. Sahoo, K. Agarwal, A. Singh, B. Polke, K. Raha, Characterization of γ - and α -Fe₂O₃ nano powders synthesized by emulsion precipitation-calcination route and rheological behaviour of α -Fe₂O₃, *Int. J. of Eng. Sci. Tech.*, (2010).
- [29] S. Ekambaram, Y. Iikubo, A. Kudo, Combustion synthesis and photocatalytic properties of transition metal-incorporated ZnO, *J. Alloys Compd.*, 433 (2007) 237-240.
- [30] M.L. Dinesha, G.D. Prasanna, C.S. Naveen, H.S. Jayanna, Structural and dielectric properties of Fe doped ZnO nanoparticles, *Indian J. Phys.*, 87 (2013) 147-153.
- [31] L. Khanna, N.K. Verma, Size-dependent magnetic properties of calcium ferrite nanoparticles, *J. Magn. Mater.*, 336 (2013) 1-7.
- [32] M.M. Ba-Abbad, A.A.H. Kadhun, A.B. Mohamad, M.S. Takriff, K. Sopian, Visible light photocatalytic activity of Fe³⁺-doped ZnO nanoparticle prepared via sol-gel technique, *Chemosphere*, 91 (2013) 1604-1611.
- [33] A.L. Patterson, The scherrer formula for x-ray particle size determination, *Phys. Rev.*, 56 (1939) 978-982.
- [34] G. Leofanti, M. Padovan, G. Tozzola, B. Venturelli, Surface area and pore texture of catalysts, *Catal. Today*, 41 (1998) 207-219.
- [35] P.P. H., JASRA Raksh V, N.B. L., B.P. N., Studies on the activity and stability of immobilized α -amylase in ordered mesoporous silicas, *Appl Catal A-Gen*, 77 (2005) 67-77.
- [36] T. Long, S. Yin, K. Takabatake, P. Zhnag, T. Sato, Synthesis and characterization of ZnO nanorods and nanodisks from zinc chloride aqueous solution, *Nanoscale Res. Lett.*, 4 (2008) 247-253.

- [37] T. Parvin, N. Keerthiraj, A.I. Ibrahim, S. Phanichphant, K. Byrappa, Photocatalytic degradation of municipal wastewater and brilliant blue dye using hydrothermally synthesized surface-modified silver-doped ZnO designer particles, *Int. J. Photoenergy*, 2012 (2012) 8.
- [38] C. Pholnak, C. Sirisathitku, S. Suwanboon, H.D. James, Effects of precursor concentration and reaction time on sonochemically synthesized ZnO nanoparticles, *Materials Research*, 17 (2014) 405-411.
- [39] R.L.M. Franco, T.G. Oliveira, A.M.G. Pedrosa, S. Naviciene, M.J.B. Souza, Textural properties of nickel, palladium and titanium oxides supported on MCM-41 materials and their application on oxidative desulfurization of dibenzothiophene, *Mater. Res.*, 16 (2013) 1448-1456.
- [40] J. Madejová, FTIR techniques in clay mineral studies, *Vib. Spectrosc.*, 31 (2003) 1-10.
- [41] C. Yu-Jin, Z. Chun-Ling, W. Li-Jiao, G. Peng, C. Mao-Sheng, S. Xiao-Ling, Synthesis and enhanced ethanol sensing characteristics of α -Fe₂O₃/SnO₂ core-shell nanorods, *Nanotechnology*, 20 (2008) 045502.
- [42] S. Karamat, R.S. Rawat, P. Lee, T.L. Tan, R.V. Ramanujan, Structural, elemental, optical and magnetic study of Fe doped ZnO and impurity phase formation, *Prog. Nat. Sci-Mater*, 24 (2014) 142-149.
- [43] Z. Jun, L. Xianghong, W. Liwei, Y. Taili, G. Xianzhi, W. Shihua, W. Shurong, Z. Shoumin, Synthesis and gas sensing properties of α -Fe₂O₃@ZnO core-shell nanospindles, *Nanotechnology*, 22 (2011) 185501.
- [44] C. Samanta, Direct synthesis of hydrogen peroxide from hydrogen and oxygen: An overview of recent developments in the process, *Appl. Catal. B-Environ.*, 350 (2008) 133-149.
- [45] X. Zhang, Y. Zhu, P. Huang, M. Zhu, Phosphotungstic acid on zirconia-modified silica as catalyst for oxidative desulfurization, *RSC Adv.*, 6 (2016) 69357-69364.
- [46] E. Yazici, H. Deveci, Factors affecting decomposition of hydrogen peroxide, *P. Int. Miner. Proces. Sym.*, Turkey, 2010.
- [47] S.L. Manatt, M.R. Manatt, On the analyses of mixture vapor pressure data: The hydrogen peroxide/water system and its excess thermodynamic functions, *Chem-Eur. J.*, 10 (2004) 6540-6557.
- [48] R.Joskić, D.Margeta, K.Sertić-Bionda, Oxidative desulfurization of model diesel fuel with hydrogen peroxide, *Goriva I Maziva Journal*, 53 (2014) 11-18.
- [49] W. Zhang, H. Zhang, J. Xiao, Z. Zhao, M. Yu, Z. Li, Carbon nanotube catalysts for oxidative desulfurization of a model diesel fuel using molecular oxygen, *Green Chem.*, 16 (2014) 211-220.
- [50] L. Cedeño-Caero, M.A. Alvarez-Amparan, Performance of molybdenum oxide in spent hydrodesulfurization catalysts applied on the oxidative desulfurization process of dibenzothiophene compounds, *React. Kinet. Mech. Cat.*, 113 (2014) 115-131.
- [51] O. Levenspiel, Chemical reaction engineering, *Ind. Eng. Chem. Res.*, 38 (1999) 4140-4143.
- [52] M. Calligaris, Structure and bonding in metal sulfoxide complexes: an update, *Coord. Chem. Rev.*, 248 (2004) 351-375.
- [53] K. Mizuno, S. Imafuji, T. Ochi, T. Ohta, S. Maeda, Hydration of the CH groups in dimethyl sulfoxide probed by NMR and IR, *J. Phys. Chem. B.*, 104 (2000) 11001-11005.
- [54] M. Shakirullah, I. Ahmad, M. Ishaq, W. Ahmad, Study on the role of metal oxides in desulphurization of some petroleum fractions, *J. Chin. Chem. Soc-Taip.*, 56 (2009) 107-114.

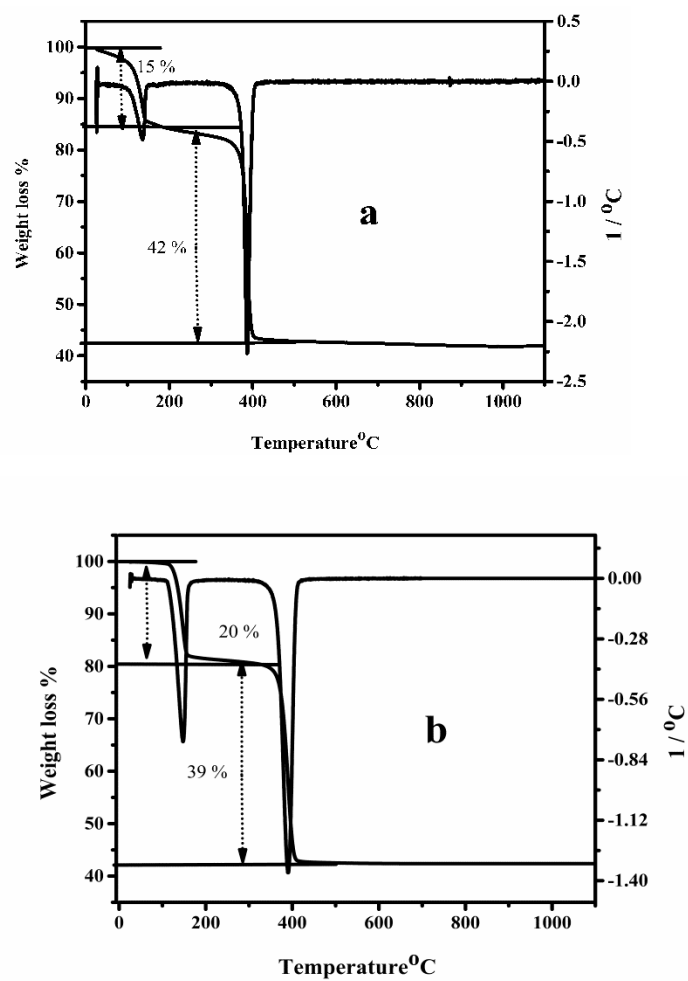


Fig. 1 TGA-DTG graphs for (a) ZnO, (b) 5 wt % Fe-ZnO

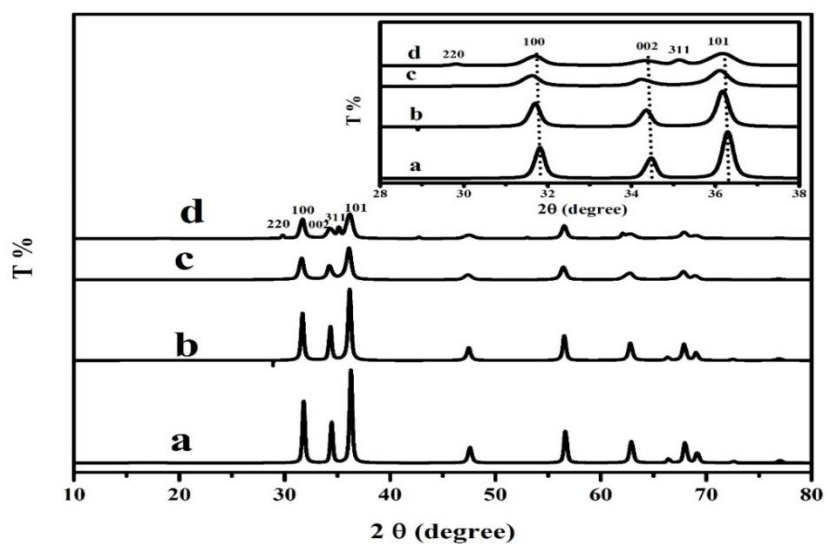


Fig. 2 XRD diffractogram of (a) ZnO, (b) 2 wt % Fe- ZnO, (c) 3 wt % Fe-ZnO, (d) 5 wt % Fe-ZnO.

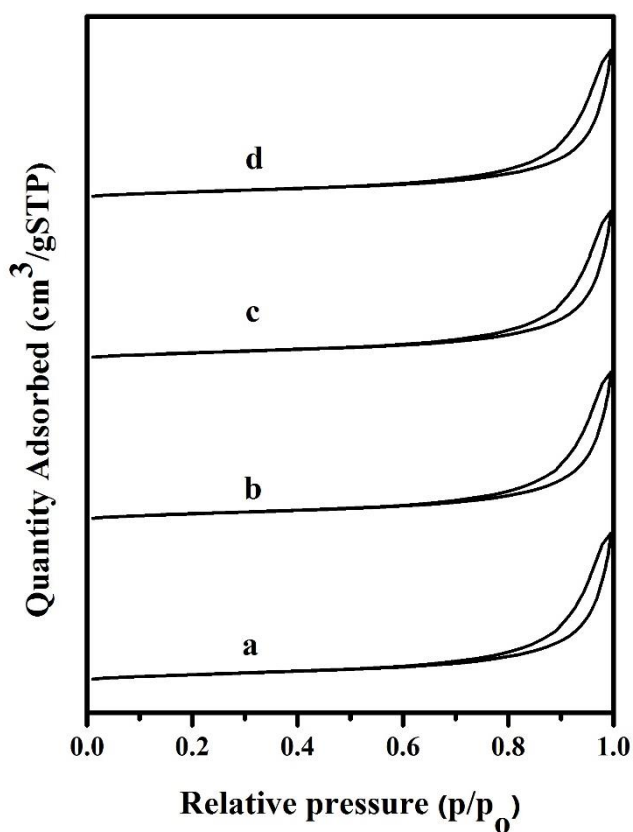


Fig. 3. N_2 adsorption-desorption isotherm of (a) ZnO, (b) 2 wt % Fe- ZnO, (c) 3 wt % Fe-ZnO, (d) 5 wt % Fe-ZnO.

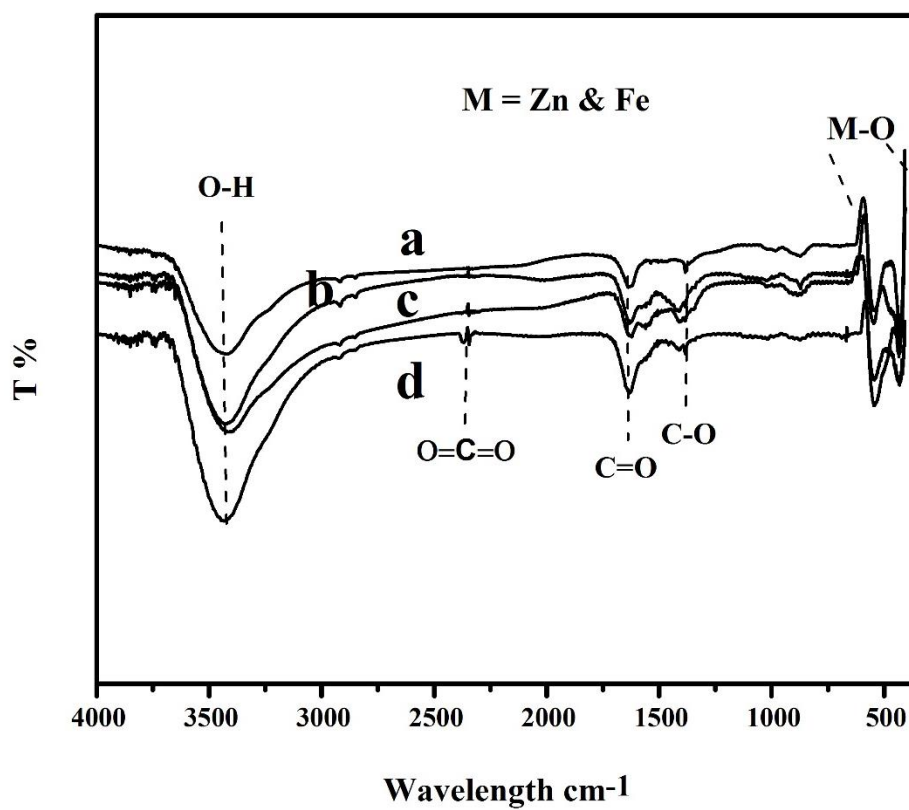
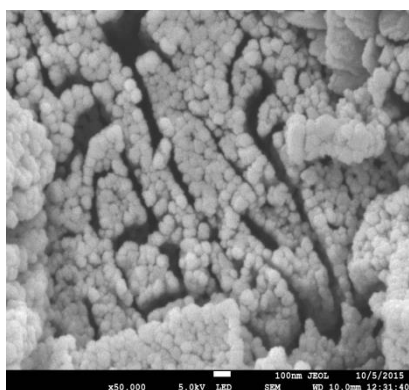
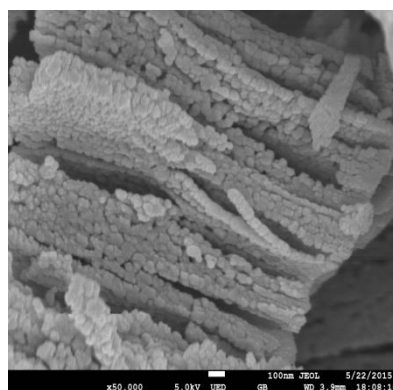


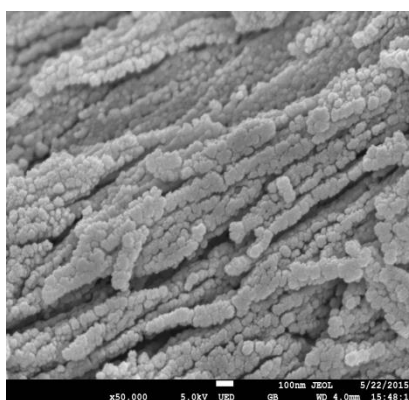
Fig. 4 FTIR spectra of (a) ZnO, (b) 2 wt % Fe-ZnO, (c) 3 wt % Fe-ZnO, (d) 5 wt % Fe-ZnO.



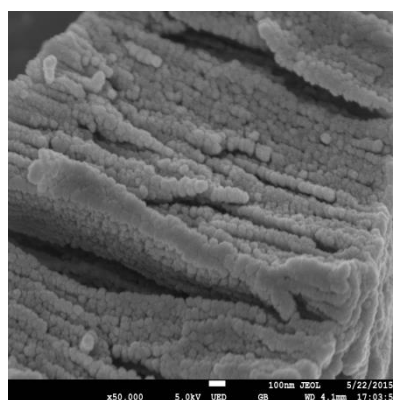
(a)



(b)



(c)



(d)

Fig. 5. FESEM micrographs of (a) ZnO, (b) 2 wt % Fe- ZnO, (c) 3 wt % Fe-ZnO, (d) 5 wt % Fe-ZnO.

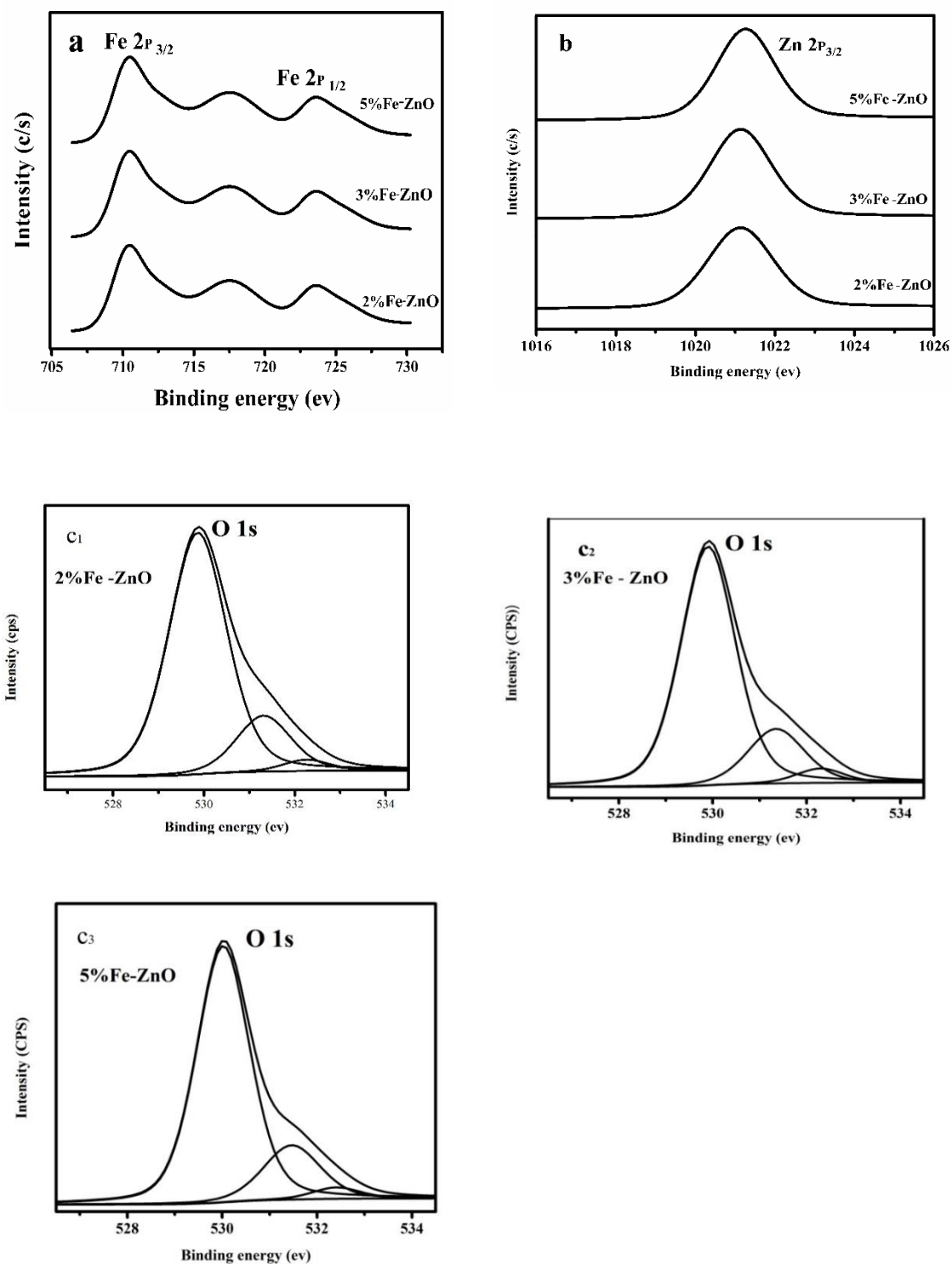


Fig. 6 (a) Fe 2p XPS of Fe-ZnO containing different amounts of Fe, (b) Zn-2p peaks of Fe-ZnO containing various amounts of Fe, (c₁, c₂, c₃) in comparison of O 1s XPS peaks Fe-ZnO with different containing amounts of Fe.

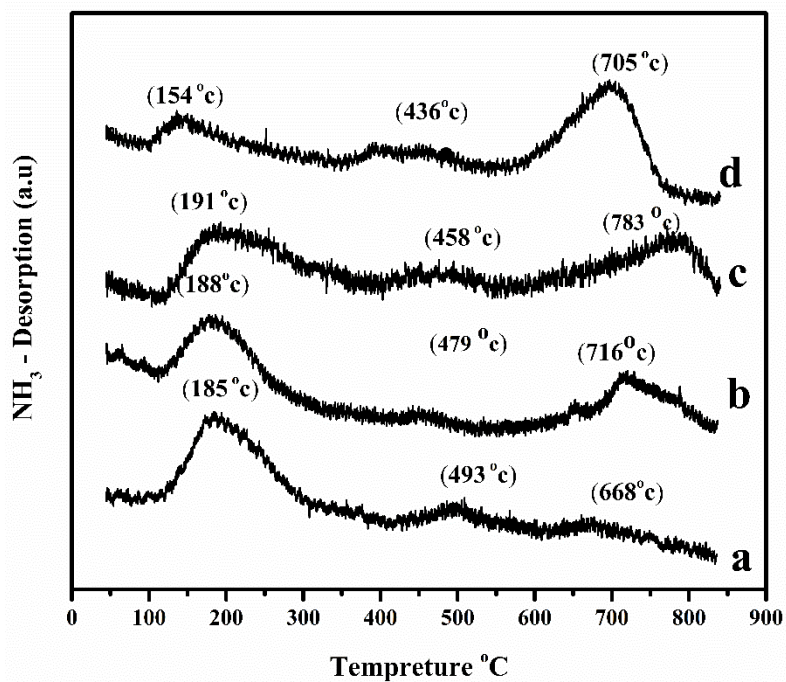


Fig. 7 NH₃-TPD analysis of (a) ZnO, (b) 2 wt % Fe-ZnO, (c) 3 wt % Fe-ZnO, (d) 5 wt % Fe-ZnO.

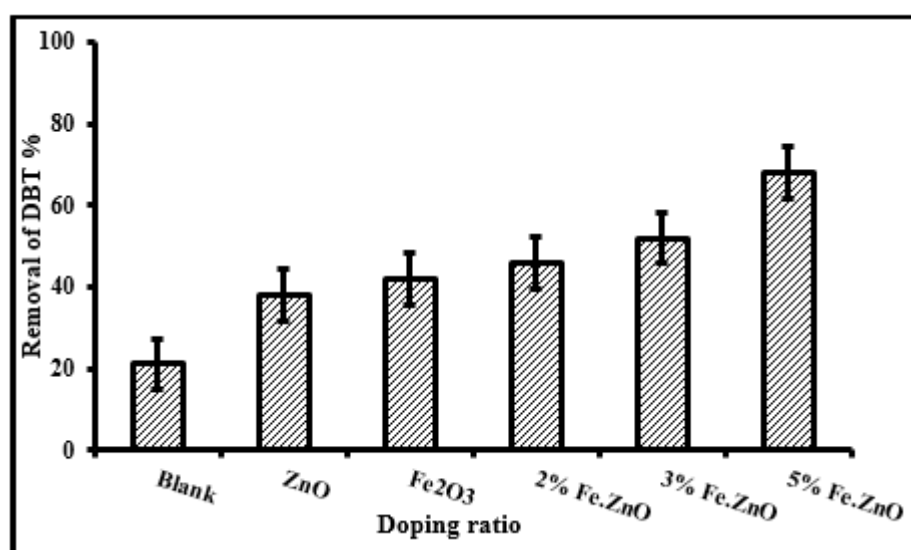


Fig. 8. Effect of Fe loading (2, 3, 5 wt %) on efficiency of DBT removal. Reaction conditions: *n*-heptane containing DBT solution, 12.5mg catalyst, O/S 2 mol ratio, 60 minutes, 80 °C, 700 rpm.

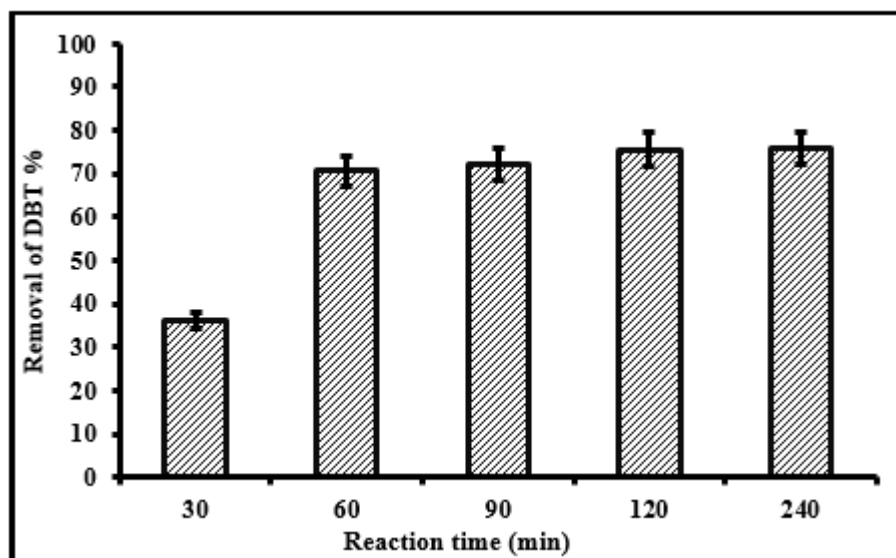


Fig. 9. Effect of reaction time on efficiency of DBT removal. Reaction conditions: *n*-Heptane containing DBT solution, 12.5 mg 5 wt % Fe-ZnO catalyst, O/S 2 mol ratio, 80 °C, and 700 rpm.

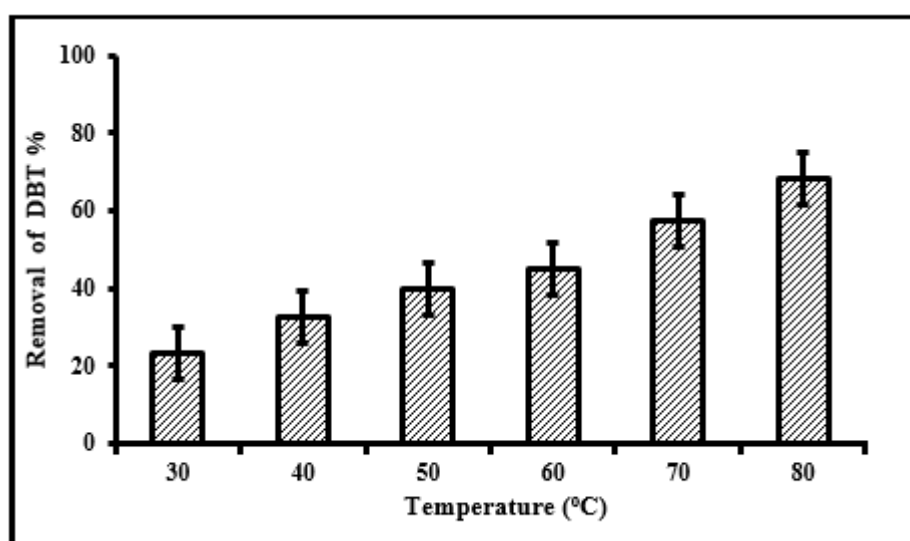


Fig. 10 Effect of reaction temperature on efficiency of DBT removal. Reaction conditions: *n*-Heptane containing DBT solution, 12.5mg 5 wt % Fe-ZnO catalyst, O/S 2 mol. ratio, 60 minutes, 700 rpm, at different temperature (30, 40, 50, 60, 70 and 80 °C).

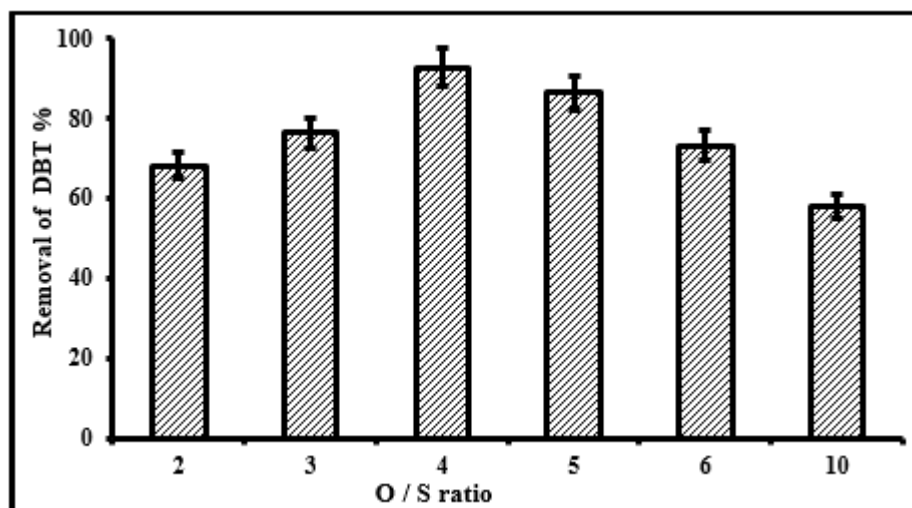


Fig. 11 Effect of O/S mol. ratio on efficiency of DBT removal. Reaction conditions: *n*-Heptane containing DBT solution, 12.5 mg 5 wt % Fe-ZnO catalyst, 60 minutes, 80 °C, 700 rpm and O/S (2, 3, 4, 5, 6, and 10) mol ratio.

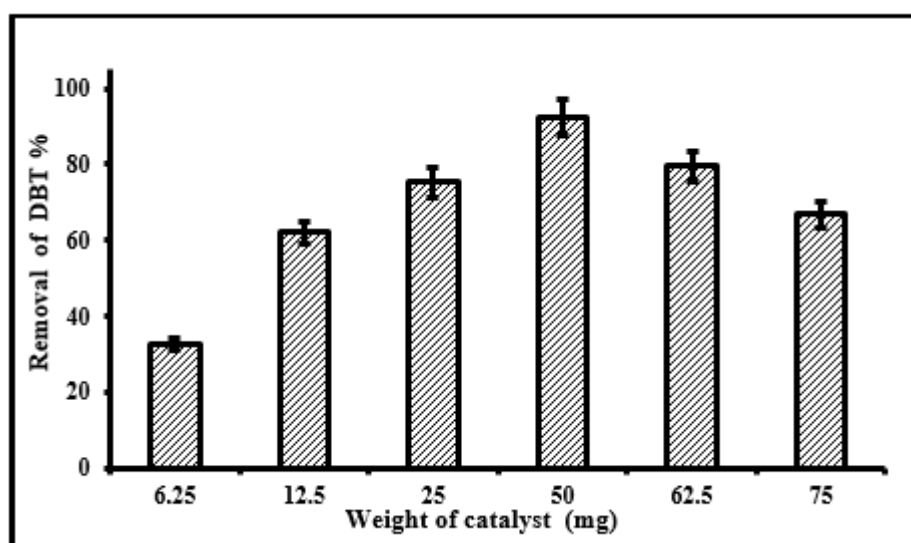


Fig. 12 Effect of catalyst mass on efficiency of DBT removal. Reaction conditions: *n*-Heptane containing DBT solution, O/S 2 mol ratio, 60 minutes, 80 °C 700 rpm, 5 wt % Fe-ZnO, (6.25, 12.5, 25, 50, 62.5, 75 mg) of catalyst.

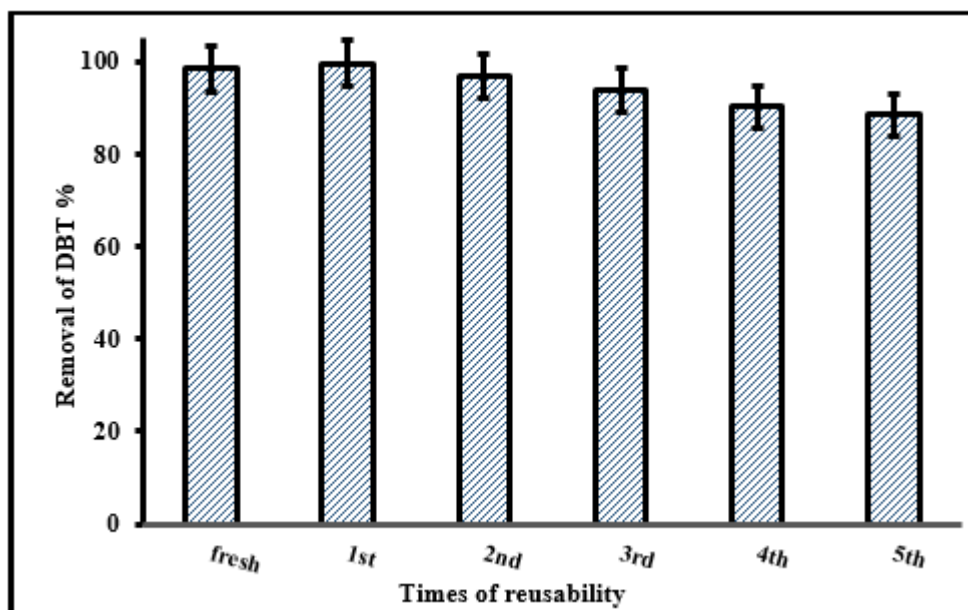


Fig. 13 Catalyst reusability study. Reaction Conditions: *n*-Heptane containing DBT solution, 50 mg of 5 wt % Fe-ZnO catalyst, O/S 4 mol ratio, 60 minutes, 80 °C and 700 rpm.

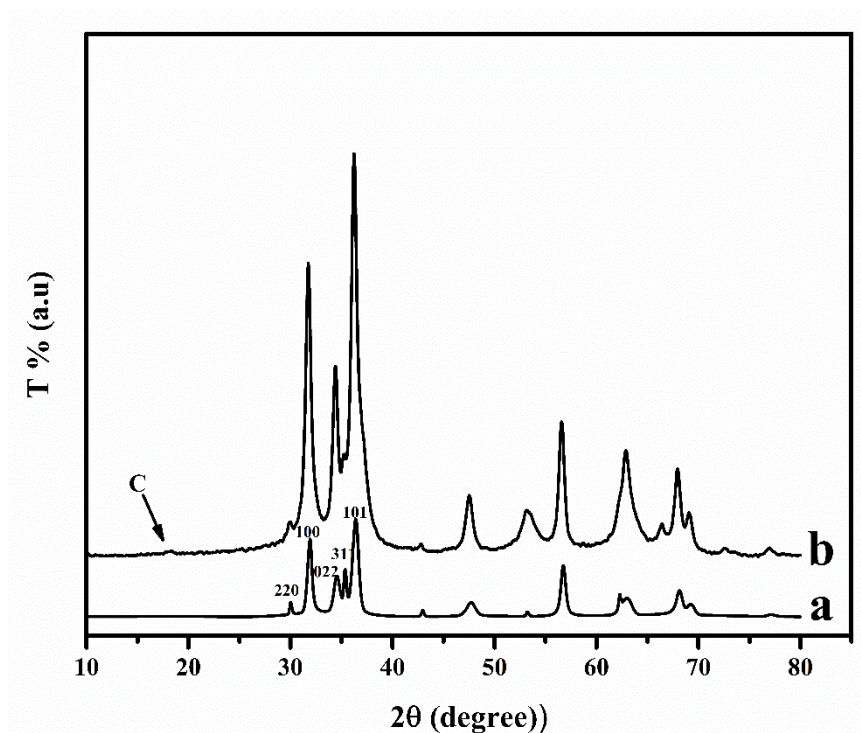


Fig. 14. XRD of (a) fresh b) spent catalyst

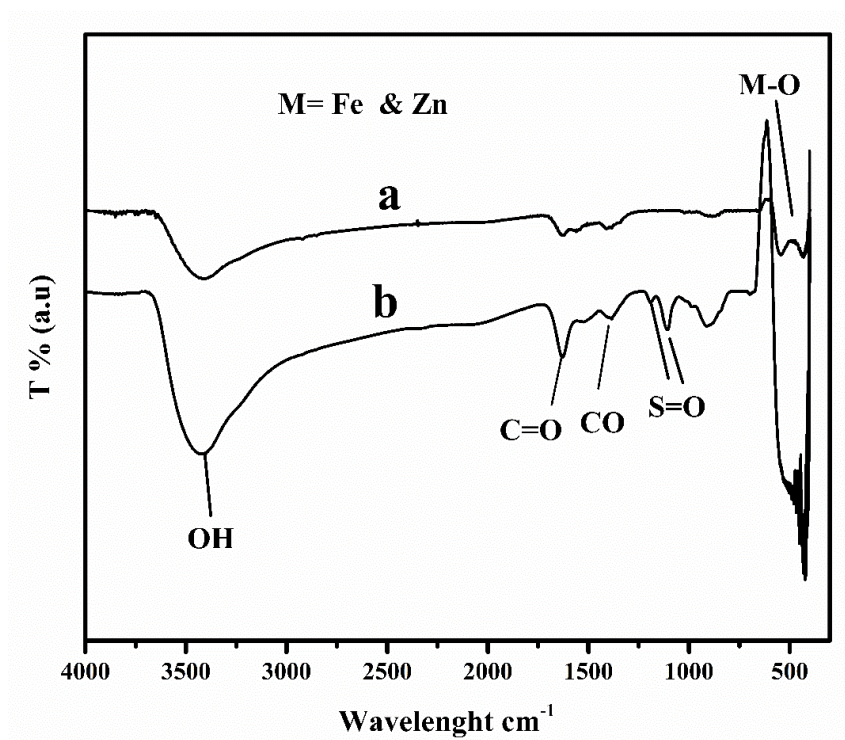


Fig. 15. FTIR spectra of (a) fresh (b) spent catalyst

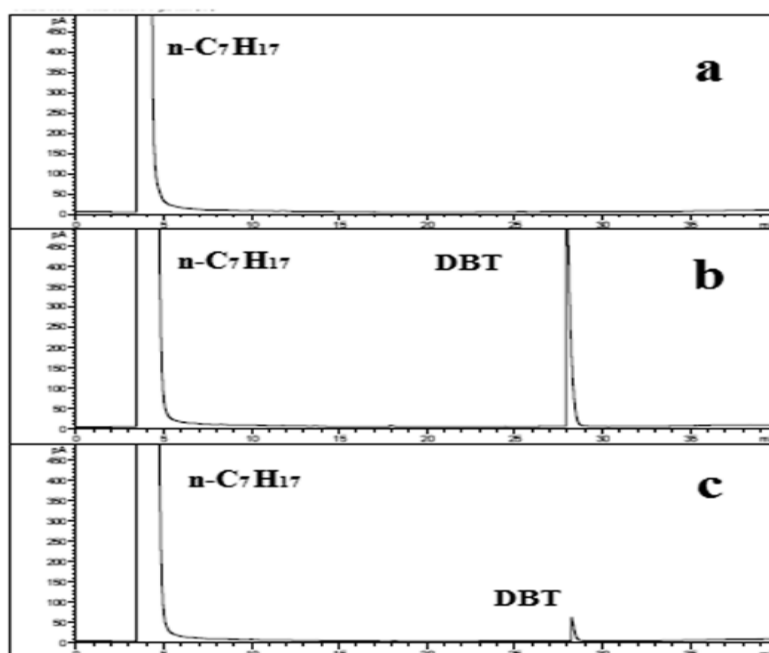


Fig. 16 (a) *n*-heptane, (b) (*n*-heptane + DBT) before ODS, (c) (*n*-heptane + DBT) after ODS

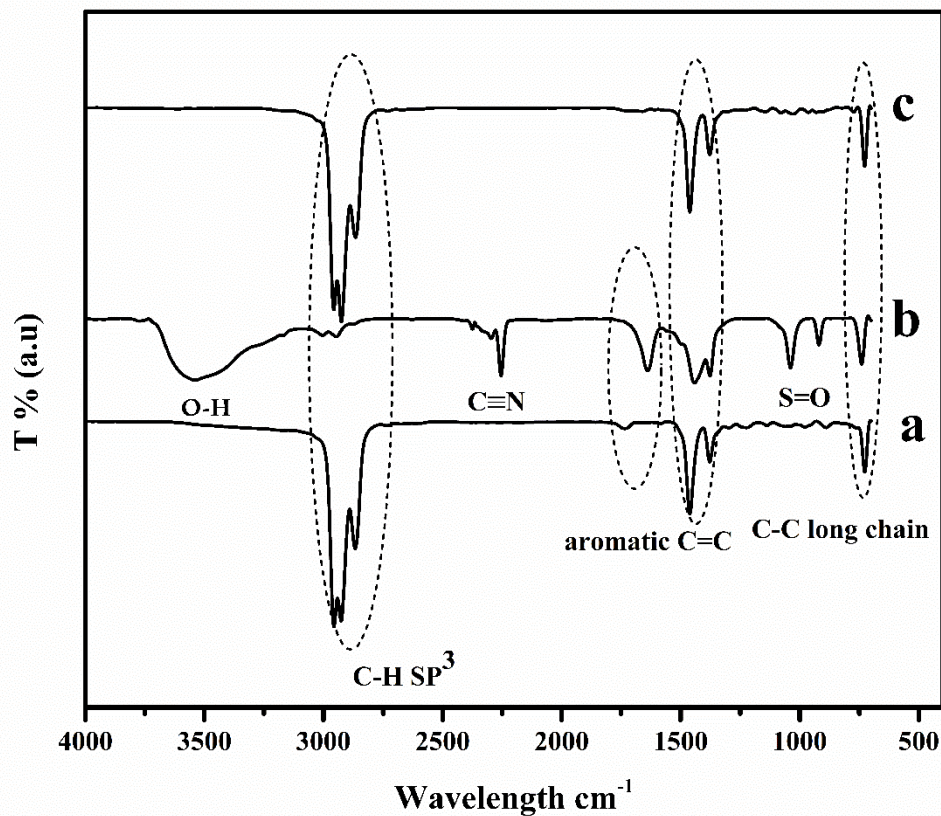
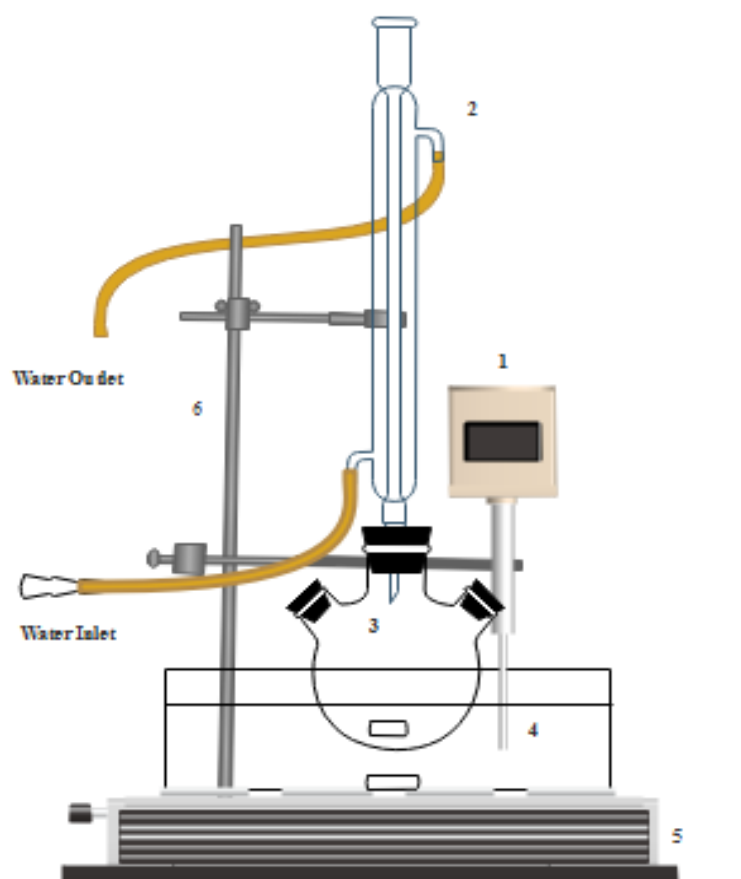
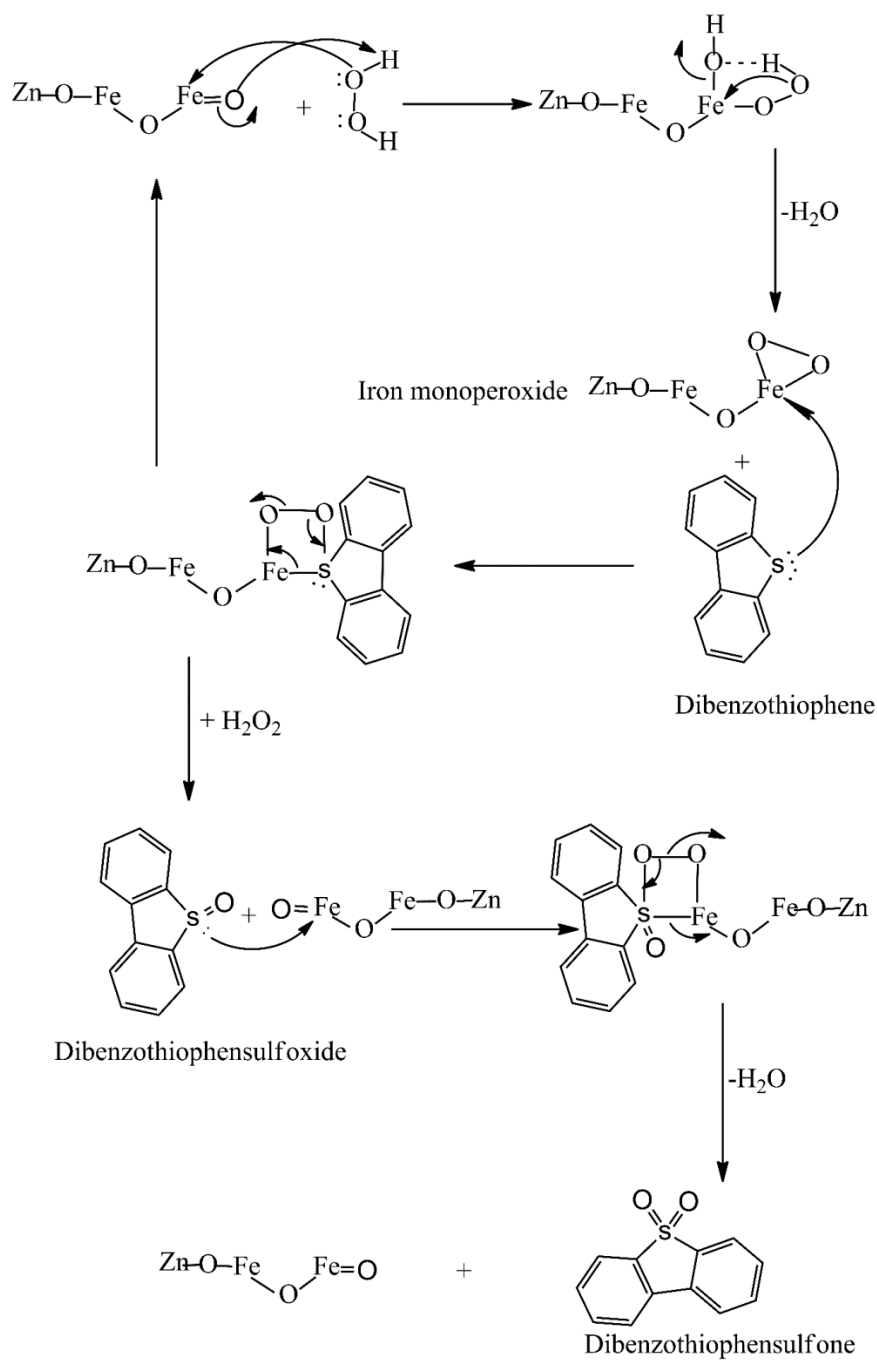


Fig. 17 (a) (*n*-heptane +DBT) simulated solution before ODS, (b) (*n*-heptane + DBT) simulated solution after ODS and before extraction, (c) (*n*-heptane + DBT) simulated solution after ODS and extraction.



Scheme.1. Catalytic testing reactor set-up. (1) Temperature controller, (2) water condenser, (3) round bottom flask, (4) Oil Bath and (5) Heating plate with stirrer controller (6) Iron stage.



Scheme.2. Propose reaction mechanism for DBT removal using H₂O₂ as oxidant and Fe-ZnO as catalyst.

Table 1

BET surface area and crystallite size of ZnO and Fe-ZnO (2, 3, 5 wt %) Fe loading.

Catalyst	BET Surface area (m ² /g)	Pore Volume (cm ³ /g)	*Crystallite size (nm)
ZnO	17.58	0.079	36
2 wt % Fe-ZnO	28.06	0.171	28
3 wt % Fe-ZnO	37.76	0.222	20
5 wt % Fe-ZnO	41.85	0.308	16

*Estimated using Scherer's formula [31];

Table 2

Energy Dispersive X-ray analysis of Fe-ZnO (2, 3, 5 wt %) Fe loading.

Catalyst	EDX (Wt. %)		
	Zn	O	Fe
2 wt % Fe- ZnO	78.93	19.20	1.87
3 wt % Fe-ZnO	77.43	20.12	2.46
5 wt % Fe-ZnO	76.88	18.92	4.20

Table 3NH₃-TPD analysis for (a) ZnO, (b) 2 wt % Fe-ZnO, (c) 3 wt % Fe-ZnO, (d) 5 wt % Fe-ZnO.

Catalyst	Amount of acid sites ($\mu\text{ mol g}^{-1}$) NH ₃				Contribution of strong acidic site (%)
	T < 200°C	200 °C < T < 400 °C	T > 400 °C	Total	
	Weak	Medium	Strong	Total	
ZnO	297.3	-	144.7	442.0	32.7
2 wt % Fe- ZnO	263.2	-	421.6	684.8	61.5
3 wt % Fe-ZnO	245.9	-	567.4	813.3	69.8
5 wt % Fe-ZnO	152.3	-	1138.4	1290.7	88.2

Table 4

BET Surface area and pore volume of fresh and spent 5 wt % Fe-ZnO catalyst.

Catalyst	BET Surface area (m ² /g)	Pore Volume (cm ³ /g)
Fresh	41.85	0.308
Spent – after 1 ODS cycle	42.45	0.178
Spent - after 6 ODS cycle	31.83	0.124